Derivation of the COS FUV Dispersion Solutions at Lifetime Position 6

William J. Fischer[1], Elaine Frazer[1], Nick Indriolo[1], Christian I. Johnson[1],
Nathaniel E. B. Kerman[1,2], Lauren P. Miller[1], and Ravi Sankrit[1]

[1] Space Telescope Science Institute, Baltimore, MD
[2] Laboratory for Atmospheric and Space Physics, Boulder, CO

13 December 2023

ABSTRACT

At strategically chosen times, the locations where spectra are obtained with particular central wavelength settings (cenwaves) on the far-ultraviolet detector of the Hubble Space Telescope's Cosmic Origins Spectrograph are changed. These locations are known as lifetime positions (LPs). At the beginning of Hubble's Cycle 30 (October 2022), LP6 became the default position for obtaining spectra with the G160M grating. At 6.5″ above the original LP in the cross-dispersion direction, the best focus value differs from that at other LPs. Therefore, new dispersion solutions are required for each affected cenwave. Here we discuss the derivation and testing of dispersion solutions for the G160M cenwaves at LP6. These were incorporated in an updated DISPTAB reference file, delivered to Hubble's Calibration Reference Data System on 2022 September 14.

Contents

1. Introduction

The far-ultraviolet (FUV) detector of the Cosmic Origins Spectrograph (COS) on the Hubble Space Telescope experiences gain sag, a position-dependent reduction in its ability to convert incoming photons into electrons with repeated use. Several strategies have been adopted to maximize the lifetime of the detector in spite of this. Among them are lifetime position (LP) moves, where the default location at which spectra are obtained with a given wavelength setting changes from time to time. Each LP has different focus values and uses a different region of the detector, so new spectral extraction parameter files, wavelength calibration files, and flux calibration files are required when a new LP is introduced.

Beginning in Cycle 30, the default LP for central wavelength settings (cenwaves) observed with the G160M grating changed from LP4 to LP6, offset in the positive direction along the cross-dispersion axis by $6.5''$ from LP1 and by $11.5''$ from LP4. LP6 has unique overheads due to the need for non-simultaneous wavelength calibration observations; see Section 9.5.1 of the COS Instrument Handbook (Soderblom et al. 2023) for more details.

This ISR is the sixth in a sequence that discusses wavelength calibration at different lifetime positions. See Plesha et al. (2018), Ake et al. (2019), Plesha et al. (2019a), Plesha et al. (2019b), and Plesha (2022) for descriptions of wavelength calibration at LP1 through LP5. It is also part of a collection of ISRs that describe the calibration of LP6. Additional LP6 calibration ISRs discuss the overall program (Sankrit et al. 2023) as well as spectral extraction (Frazer et al., in prep.), lamp templates (Indriolo et al. 2023), flat fields and flux calibration (Miller et al., in prep.), gain maps (Johnson & Sahnow 2023), and the spectral and spatial resolution at LP6 (Kerman et al. 2023b, 2023a).

2. Observations

The dispersion solutions at LP6 were derived from spectra of the nearby K2V dwarf star ϵ Eri. This star is chromospherically active and thus has many FUV emission lines that can be used for wavelength calibration. Additionally, it has been used for wavelength calibration at previous LPs. Therefore, it is well understood which lines

Table 1.   Structure of Program 16908

Cenwave	Visit	Exp. Time (s)	Start Time (UT)	Dataset	Exposure
1533	01	2400.2	2022-03-07 02:17	let801020	let801bgq
1577	01	2400.2	2022-03-07 03:53	let801030	let801c1q
1589	01	1777.2	2022-03-07 00:55	let801010	let801amq
1600	02	2400.2	2022-03-08 08:28	let802020	let802gfq
1611	02	1771.2	2022-03-08 07:05	let802010	let802g9q
1623	02	2400.2	2022-03-08 10:03	let802030	let802gwq

vary significantly due to chromospheric activity, and the few that do can be excluded from use in wavelength calibration (Plesha et al. 2019a).

Program 16908 (COS FUV LP6 Calibration: Dispersion Solutions; PI W. Fischer) observed the star with all six G160M cenwaves in two visits of three orbits each. Visit 01, covering cenwaves 1533, 1577, and 1589, ran on 7 March 2022. Visit 02, covering cenwaves 1600, 1611, and 1623, ran the day after. Each visit began with a double ACQ/IMAGE target acquisition with the Bright Object Aperture and Mirror B. Each acquisition exposure was 25 s in length. Double acquisitions ensure improved target centering for the zero-point measurements. In an analysis of acquisitions in the LP3 wavelength calibration program (PID 14909), double ACQ/IMAGEs were confirmed to center the target 2 to 3 times more accurately than single ACQ/IMAGEs (Plesha 2017).

Exposure times were driven by the number of counts needed to achieve accurate cross-correlations using multiple emission lines. We aimed to achieve at least S/N $\sim$ 5 in the peaks of weak emission lines. Using the line at 1681.2 Å as the fiducial weak line for ETC calculations, we found that 2031 to 2369 s were needed per cenwave, increasing for longer wavelengths.

For cenwaves 1533, 1577, 1600, and 1623, these exposure times were extended to 2400 s to nearly fill the orbit. (In Cycle 30, LP6 exposure times longer than 2400 s were not recommended due to the potential for reduced wavelength calibration accuracy; see Rowlands et al., in prep.) Cenwaves 1589 and 1611 share their orbits with the acquisition sequence and were observed for 1777 or 1771 s, respectively, resulting in 90% of the requested S/N. This is acceptable because their dispersion coefficients are informed, in part, by interpolating from those of adjacent cenwaves in either direction.

Spectra were obtained with both detector segments on at FP-POS 3 only. All spectroscopic exposures were preceded and followed by split-wavecal exposures, as is the default at LP6. Table 1 lists details about the exposures for this program.

3. Data Reduction

The relevant `rawtag` files for ϵ Eri were processed with CalCOS (v3.4.3). We used TWOZONE extraction based on newly created reference files for LP6. These included the XTRACTAB, PROFTAB, TRACETAB, and TWOZXTAB. Further, an updated BPIXTAB was used. For the initial wavelength calibration, the LP4 DISPTAB was used alongside a newly created LAMPTAB (Indriolo et al. 2023). This was judged appropriate because the cross-correlation procedure described in Section 4 produces reliable dispersion solutions if the initial coefficients are reasonably close to the final ones. This was expected to be the case for LP6 versus LP4, and this assumption was verified to be reasonable when testing the final result (Section 5). Because we do not need precise fluxes for wavelength calibration, we also used the LP4 FLUXTAB and FLATFILE and did not attempt to correct for time-dependent sensitivity (TDSCORR = OMIT). RANDSEED was set to 7654321 to facilitate comparison among different calibration runs. All other calibration switches were left at their defaults.

4. Deriving the Dispersion Solutions

As has been the case for all medium resolution COS modes at all previous LPs, we derived linear dispersion solutions for the G160M cenwaves at LP6. The zero points (in Å) are contained in the first coefficient of the COEFF column of the DISPTAB, and the dispersion constants (in Å px^{-1}) are contained in the second coefficient. The columns D and D_TV03 were set to zero; these were useful in the past when dispersion solutions were determined with reference to data obtained during thermal vacuum testing (Oliveira et al. 2010).

Data for multiple COS apertures may be included in a DISPTAB: the primary science aperture (PSA), the wavelength calibration aperture (WCA), and the bright object aperture (BOA). Here we discuss the calculation of entries for the G160M gratings through the PSA. Entries for other gratings through the PSA and for all gratings through the WCA were left at the values present in the LP4 DISPTAB. The LP6 DISPTAB contains no entries for the bright object aperture (BOA), because the BOA cannot be used at LP6. Fischer et al. (2022) discuss the problems inherent in attempting to use the BOA at LP5 and above on the detector.

Similarly to previous wavelength calibration efforts, the dispersion solutions were determined by cross-correlating COS data with STIS E140M data. This is effective because of the superior wavelength accuracy of STIS relative to COS. The STIS E140M dispersion solutions have an absolute accuracy of 3.3 km s^{-1} (Prichard et al. 2022). In contrast, for the COS FUV G130M and G160M gratings, we aim for an accuracy of 7.5 km s^{-1} (Soderblom et al. 2023). The STIS spectra for ϵ Eri came from Programs 7479 and 13650. STIS data were convolved with the expected COS line-spread function at LP6 (Kerman et al. 2023b).

For each cenwave and segment, the spectra were cross-correlated in small

windows of up to 3.2 Å in width that contained from one to six emission lines. Light curves were plotted for each window with data from the `corrtag` files, and windows containing variable lines, e.g., C IV λ1550, were excluded from the analysis. See Plesha et al. (2019a) for a discussion of which lines in the G160M range are useful and which are variable. Windows at XCORR pixel values less than 1500 were also excluded from the analysis. This region of the detector suffers from large walk and geometric distortions, which is currently being addressed in COS calibration work. The cross-correlation results were used to generate tables of pixel shifts versus wavelength for each cenwave and segment. These were fit with straight lines; the intercept and slope of each line were the preliminary entries for the DISPTAB.

It is expected that the dispersion coefficients (the slopes of the best-fit lines) increase linearly with focus. This is because a positive change in focus moves the grating closer to the detector, causing each pixel to cover a larger wavelength range (Ake et al. 2019). Figure 1 plots the slopes versus focus. For LP1 through LP4, the values from the delivered DISPTABs are shown and connected by their best-fit lines. (G160M has never been used at LP5.) For LP6, the preliminary values determined with the method described in the preceding paragraph are shown.

As was done at previous LPs, we replaced the LP6 dispersion coefficients for cenwaves 1577 through 1623 with values that were found by fitting the lines displayed in Figure 1 to the preliminary coefficients. The slopes of the lines were fixed at the values found from ray-trace modeling of LP2, the closest LP along the cross-dispersion direction for which such model slopes had been calculated at the time of analysis. The intercepts of the lines were found by fitting lines with those slopes to the preliminary dispersion coefficients. Cenwave 1533 is significantly offset from the others and may not follow the expected linear relationship, so its dispersion coefficient was not modified in this way, which was also the case for LP4. For cenwaves 1577 through 1623, the zero points were then recalculated by fitting the pixel shifts versus wavelength with lines whose slopes were fixed to the dispersion coefficients derived from ray-trace modeling.

After the redetermination of dispersion coefficients, the residuals were calculated for each window. Figure 2 plots the residual pixel shifts versus wavelength for each combination of cenwave and segment. Four segments had one or two windows with large residuals that were excluded from the fitting. Because they are all fairly close to the edges of their respective segments, they likely suffer from large walk or geometric distortion but were not excluded in the previously mentioned XCORR cut. The standard deviation in each case is less than 3 pixels, which is the error goal for the COS medium-resolution modes. Table 2 lists the adopted zero points and dispersion coefficients.

Similar to previous derivations of wavelength solutions, we attempted to iterate to improve the results. Cross-correlation shifts are more accurate when the offsets are small, which may lead to smaller residuals upon iteration. The initially derived dispersion relations were used to calibrate the data, then the dispersion relations were re-derived. For the LP6 dispersion solutions, the residuals, which were already within specifications, did not improve. We believe this is because the initial LP4 solution was
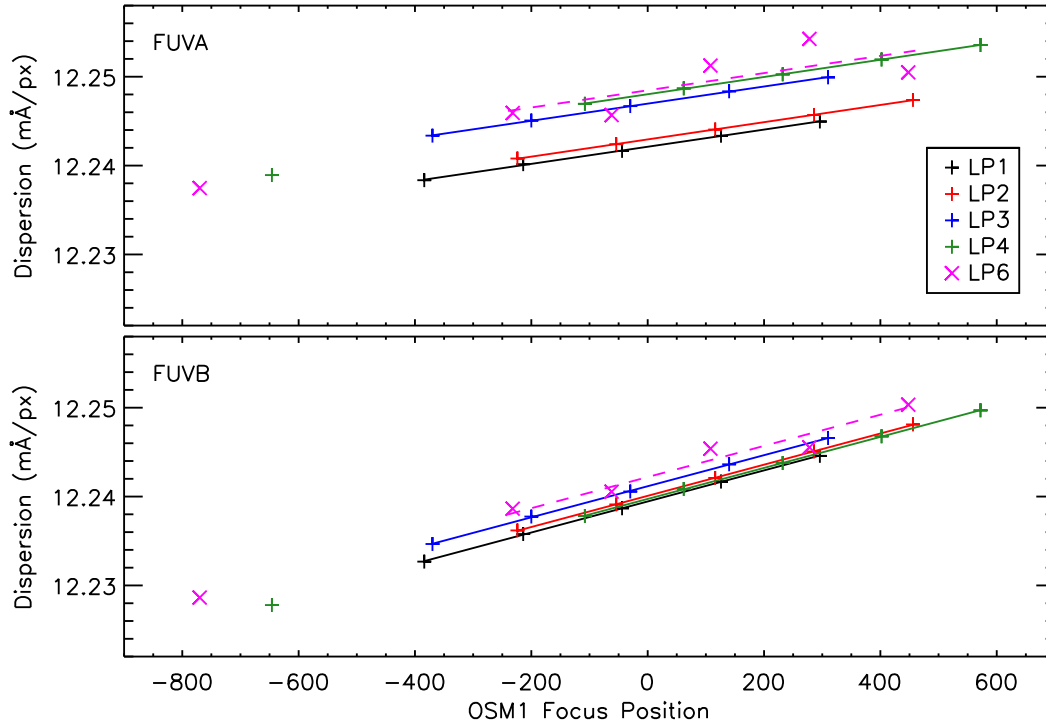
Figure 1. Dispersion versus focus for the G160M cenwaves at each LP. Cenwaves increase with increasing focus. For LP1 through LP3, all dispersion values are chosen such that they fall along lines with slopes predicted by ray-trace models. This is also the case for LP4, except cenwave 1533 (focus −646), which was introduced at LP4, has a substantially different focus from the others and is not expected to follow the relationship. At LP6, the measured dispersions are shown. In the DISPTAB, the dispersions for all cenwaves except 1533 are replaced with those that follow the best-fit line. Note that G160M cenwaves have never been available at LP5.
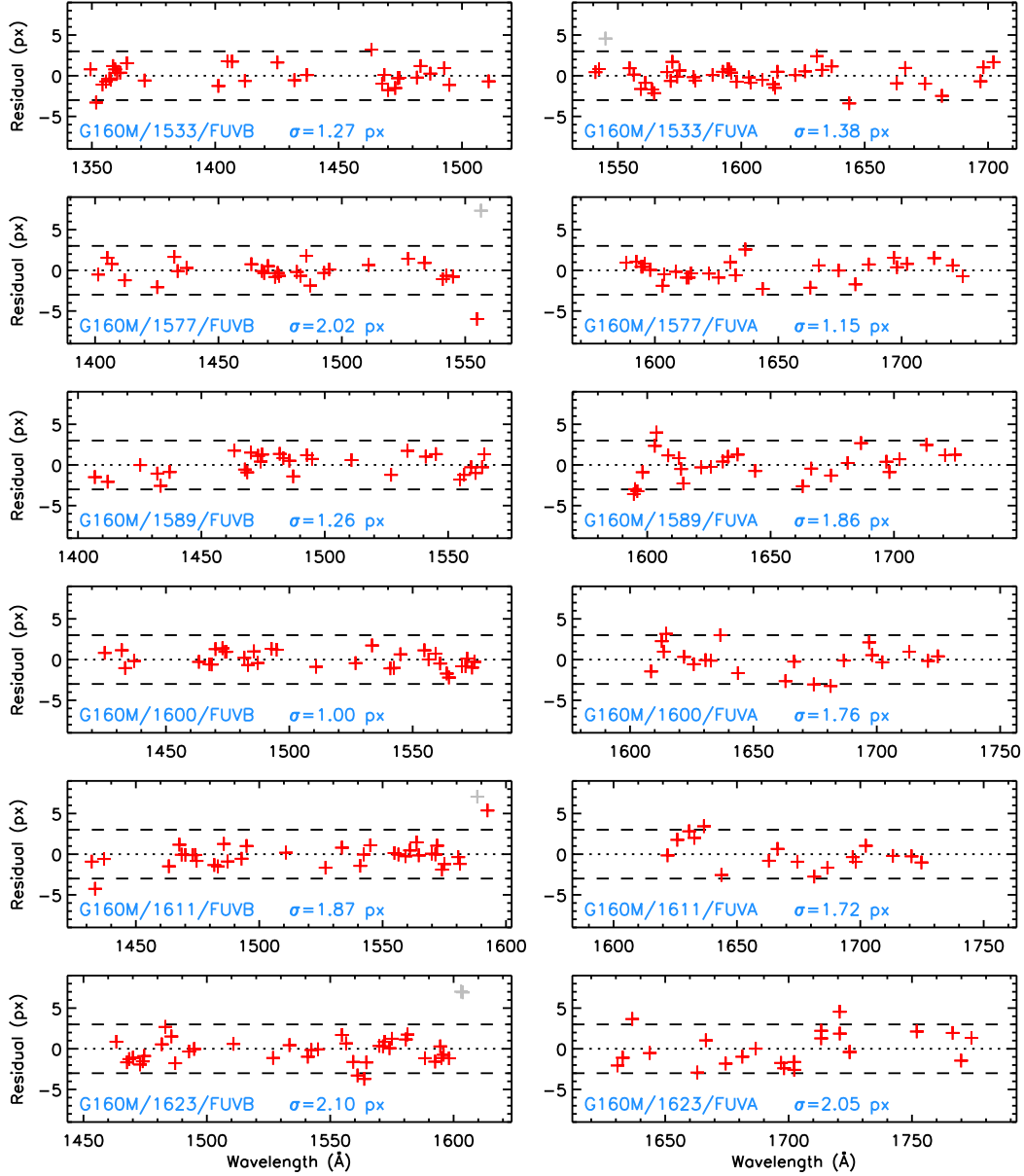
Figure 2. Plots of residual pixel offset versus wavelength for line centroids measured in each G160M cenwave and segment. Dashed lines show the 3-pixel error goal for the COS medium-resolution modes. Gray points are outliers excluded from the fitting; see the text for details. The standard deviation of the residuals is shown in each panel.

Table 2.   LP6 DISPTAB Entries[1]

Cenwave	FUVB		FUVA	
	Zero Point[2] (Å)	Dispersion (mÅ px^{-1})	Zero Point[2] (Å)	Dispersion (mÅ px^{-1})
1533	1330.2364	12.2286	1518.2468	12.2375
1577	1374.2665	12.2381	1562.4023	12.2462
1589	1385.9204	12.2411	1574.1104	12.2479
1600	1397.3114	12.2441	1585.5481	12.2495
1611	1409.1231	12.2471	1597.4104	12.2512
1623	1421.2655	12.2501	1609.6003	12.2528

[1]For clarity of presentation, the number of significant figures is limited. See the LP6 DISPTAB (`69d2109fl_disp.fits`) for full-precision values. All entries are for the PSA.

[2]Wavelength at pixel 0 (FP-POS = 3). For FUVA, the active area begins at XCORR pixel 1060; for FUVB, it begins at XCORR pixel 809.

already sufficiently close to the LP6 solution; therefore, the cross-correlation results were already as accurate as possible.

5. Testing the Dispersion Solutions

Before the beginning of Cycle 30, LP6 had been used for only a small number of calibration programs; thus, limited data are available for testing. We proceed by checking the wavelength calibration for two stars: ε Eri and AV 75. Results are shown in Figure 3.

5.1 ε Eri

With an accurate dispersion solution, there should be good agreement between features in overlapping segments and cenwaves of a given observation of a star. For ε Eri, the top panel of Figure 3 shows the offsets between lines based on a cross-correlation analysis when the same wavelength window appears in different settings of the LP6 observations (PID 16908). All possible overlaps were used, except we avoid comparing a segment to itself or comparing one segment to another when the reverse comparison has already been made. Gray symbols can refer to cases where one window or the other appears below pixel 3000 or above pixel 14000. In this case, the window is near the edge of one

cenwave or the other, where walk and geometric distortions are currently large enough to yield poor alignment in some cases. (Recall that windows below pixel 1500 were excluded from the analysis entirely due to larger distortions there.) Gray symbols can also refer to cases where the peak of the cross-correlation function is less than 0.8. This means the lines in one window or both windows suffer from a poor signal-to-noise ratio. Even in these cases, shifts are rarely more than a few pixels. In cases marked by red symbols, where both windows are far from the edges of their wavelength ranges and the cross-correlation peak is close to one, the standard deviation of all windows is 1.5 pixels, less than the 3 pixel requirement.

The second panel of Figure 3 compares ϵ Eri spectra from the LP6 program to ϵ Eri spectra from the LP4 dispersion solution program, Program 15365 (COS FUV Dispersion Solutions at LP4; PI R. Plesha). Gray symbols and red symbols have the same meaning as above. In this case, the standard deviation of all good windows is 1.6 pixels, again less than the 3 pixel requirement.

5.2 AV 75

AV 75 is the other star observed during LP6 calibration that has a significant number of lines, in Program 16907 (Mapping the COS LP6 Spectral Resolution; PI N. Kerman). It is an O5.5 supergiant in the Small Magellanic Cloud. Absorption lines that formed along the line of sight to the star have been routinely used in the past to monitor the stability of the COS FUV wavelength solutions (e.g., by Fischer et al. 2022).

Like with ϵ Eri, there should be good agreement between overlapping segments and cenwaves of a given observation of a star, and also among spectra of the same star observed at different times and lifetime positions. The third panel of Figure 3 shows the offsets between lines based on a cross-correlation analysis when the same wavelength window appears in different settings of the LP6 observations. Program 16907 obtained spectra only at cenwaves 1533 and 1623, so there are only a few windows with overlap. The good windows, as defined in the previous subsection, have a standard deviation of 1.0 pixels, less than the 3 pixel requirement.

The final test is to compare spectra of AV 75 obtained at LP6 to those obtained of the same star at LP4 in Program 16534 (Cycle 29 COS FUV Wavelength Scale Monitor; PI W. Fischer). In this case, the overlap between cenwave 1533 observed at LP6 and cenwave 1577 observed at LP4 allows for more points of comparison than in the immediate previous test, but many of the windows occur near the edges of one cenwave or the other. The fourth panel of Figure 3 shows that the good windows, as defined above, have a standard deviation of 0.9 pixels, less than the 3 pixel requirement.

Based on limited data, we conclude from these four tests that the G160M dispersion solutions at LP6 achieve the required accuracy.
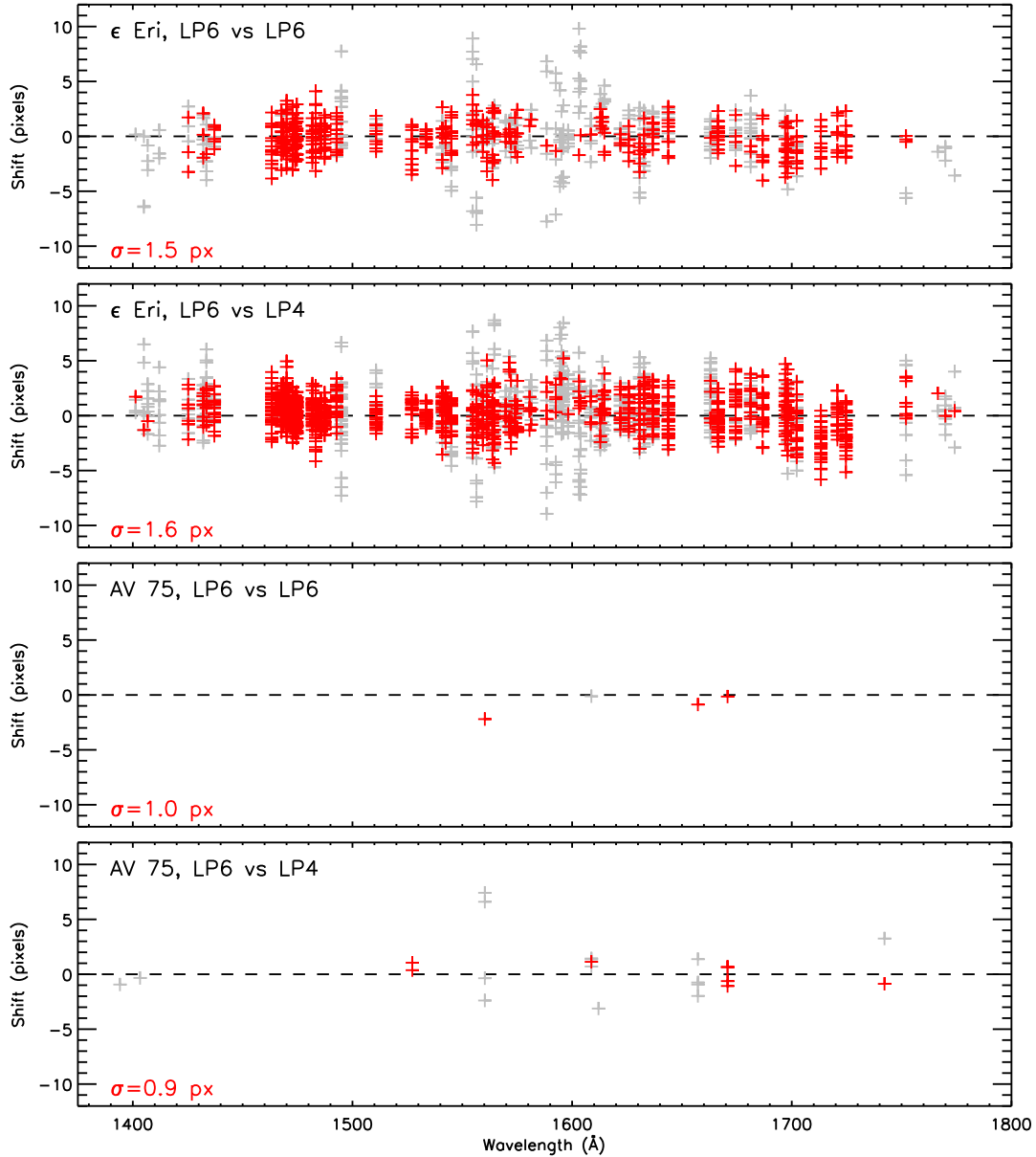
Figure 3. Cross-correlation shifts from the four tests described in Section 5. The top panel compares different cenwaves and segments of the LP6 ε Eri data. The second panel compares LP6 spectra of ε Eri to LP4 spectra of the same star. The third panel compares different cenwaves and segments of the LP6 AV 75 data. The fourth panel compares LP6 spectra of AV 75 to LP4 spectra of the same star. In all cases, red symbols represent good windows, where both windows are reasonably far from the edge of the spectrum and the cross-correlation peak exceeds 0.8.

6. Summary

COS spectra of the emission-line star ϵ Eri were obtained with all G160M cenwaves at LP6 and used to determine linear dispersion solutions. These were incorporated into an updated DISPTAB reference file, `69d2109fl_disp.fits`, which was delivered to Hubble's Calibration Reference Data System on 2022 September 14.

Change History for COS ISR 2023-28

Version 1: 13 December 2023 – Original Document

References

Ake, T., Plesha, R., De Rosa, G., et al. 2019, COS ISR 2018-23, "Improvements to the COS FUV G130M and G160M Wavelength Solutions at Lifetime Position 2"

Fischer, W. J. 2022, COS ISR 2022-10, "Cycle 28 COS FUV Wavelength Scale Monitor"

Fischer, W. J., Dieterich, S., Frazer, E. M., et al. 2022, COS ISR 2022-03, "Summary of COS Calibration for the Lifetime Position 5 Era"

Indriolo, N., Fischer, W., Frazer, E., et al. 2023, COS ISR 2023-09, "Creation of the LAMPTAB Reference File for Use at Lifetime Position 6"

Johnson, C. I., & Sahnow, D. 2023, COS ISR 2023-07, "COS FUV Detector Gain Maps Obtained at the Start of LP6 Operations"

Kerman, N. E. B., Frazer, E., Sahnow, D., et al. 2023a, COS ISR 2023-04, "The G160M Spatial Resolution of the COS FUV Channel at Lifetime Position 6"

Kerman, N. E. B., Sahnow, D., James, B., et al. 2023b, COS ISR 2023-02, "The G160M Spectral Resolution of the COS FUV Channel at Lifetime Position 6"

Oliveira, C., Béland, S., Keyes, C., & Niemi, S. 2010, COS ISR 2010-06, "SMOV: COS FUV Wavelength Calibration"

Plesha, R. 2017, HST Proposal, Cycle 24, 15365

Plesha, R. 2022, COS ISR 2022-02, "Derivation of the COS FUV Wavelength Dispersion Solution at Lifetime Position 5"

Plesha, R., Ake, T., De Rosa, G., et al. 2018, COS ISR 2018-22, "Improvements to the COS FUV G130M and G160M Wavelength Solutions at Lifetime Position 1'

Plesha, R., Ake, T., De Rosa, G., Oliveira, C., & Penton, S. 2019a, COS ISR 2018-24, "Improvements to the COS FUV G130M and G160M Wavelength Solutions at Lifetime Position 3"

Plesha, R., Ake, T., De Rosa, G., Oliveira, C., & Penton, S. 2019b, COS ISR 2018-25, "Improvements to the COS FUV G130M and G160M Wavelength Solutions at Lifetime Position 4"

Prichard, L., Welty, D., Jones, A., et al. 2022, *Space Telescope Imaging Spectrograph Instrument Handbook*, Version 21.0 (Baltimore: STScI)

Sankrit, R., Fischer, W., Frazer, E., et al. 2023, COS ISR 2023-25, "Overview of COS Lifetime Position 6 Calibration"

Soderblom, D. R., et al. 2023, *Cosmic Origins Spectrograph Instrument Handbook*, Version 15.0 (Baltimore: STScI)